Development of High-Frame Rate Neutron Radiography and Quantitative Measurement Method for Multiphase Flow Research

K. Mishima and T. Hibiki
Research Reactor Institute, Kyoto University
Kumatori-cho, Sennan-gun, Osaka 590-04 Japan

ABSTRACT

Neutron radiography (NR) is one of the radiographic techniques which makes use of the difference in attenuation characteristics of neutrons in materials. Fluid measurement using the NR technique is a non-intrusive method which enables visualization of dynamic images of multiphase flow of opaque fluids and/or in a metallic duct. To apply the NR technique to multiphase flow research, high frame-rate NR was developed by combining up-to-date technologies for neutron sources, scintillator, high-speed video and image intensifier. This imaging system has several advantages such as a long recording time (up to 21 minutes), high-frame-rate (up to 1000 frames/s) imaging and there is no need for a triggering signal. Visualization studies of air-water two-phase flow in a metallic duct and molten metal-water interaction were performed at recording speeds of 250, 500 and 1000 frames/s. The qualities of the consequent images were sufficient to observe the flow pattern and behavior. It was also demonstrated that some characteristics of two-phase flow could be measured from these images in collaboration with image processing techniques. By utilizing geometrical information extracted from NR images, data on flow regime, bubble rise velocity, and wave height and interfacial area in annular flow were obtained. By utilizing attenuation characteristics of neutrons in materials, measurements of void profile and average void fraction were performed. It was confirmed that this new technique may have significant advantages both in visualizing and measuring high-speed fluid phenomena when other methods, such as an optical method and X-ray radiography, cannot be applied.

1. INTRODUCTION

Neutron radiography (NR) is one of the radiographic techniques which makes use of the difference in attenuation characteristics of neutrons in materials [1]. Since thermal neutrons easily penetrate heavy materials like dense metals and are attenuated well by light materials as those containing hydrogen, NR has complementary performance characteristics to X-ray radiography and was developed as a technique for nondestructive inspection in the automobile and aerospace industries [2]. Recently, the application has spread to various scientific fields such as agricultural, medical and dental sciences, as well as application to porous materials like concrete and brick. Moreover, the dynamic imaging method of NR, namely the real-time NR, has been demonstrated to be a very useful tool for fluid research because this non-intrusive technique is suitable for visualization of a multiphase flow in a metallic casing [3-12] or of opaque fluids such as liquid metal [13].

However, since the recording speed of widely used imaging systems for real-time NR is 30 frames/s, the application has been restricted to the visualization of relatively slow phenomena and measurements of time-averaged quantities. Usually, a recording speed faster than about 500 frames/s is required to visualize fluid phenomena in which fluid particles move rapidly, this restriction can be a fatal shortcoming in applying it to fluid research. For this reason, a high-frame-rate NR with a pulsed neutron beam was invented to overcome this limitation [7,19,20]. Although the recording speed of approximately 10,000 frames/s could be achieved by using a pulsed neutron beam [19], this method has such problems that the recording time is very short, a triggering signal is needed to start recording in accordance with the pulse and the neutron flux, consequently the brightness of the image, varies rapidly with time. When both high-frame-rate and long recording time are required, a high-frame-rate NR with a steady neutron beam is needed instead of NR with a pulsed neutron beam. Recently, some research reactors [21,22] with a steady neutron flux over 10^8 n/cm^{2}s and highly sensitive imaging devices [23] have become available for NR, which enabled development of a high-frame-rate NR system with a steady neutron beam. In the last several years, our research group has been challenging to develop a high-frame-rate NR system by combining up-to-date technologies for neutron source, scintillator, high-speed video and image intensifier, for the visualization and measurement of rapid fluid phenomena.

In addition to the development of a high-frame-rate NR system, the development of a method for quantitative measurements is necessary, since with spreading application fields, it is thought that the research trend is changing from qualitative to

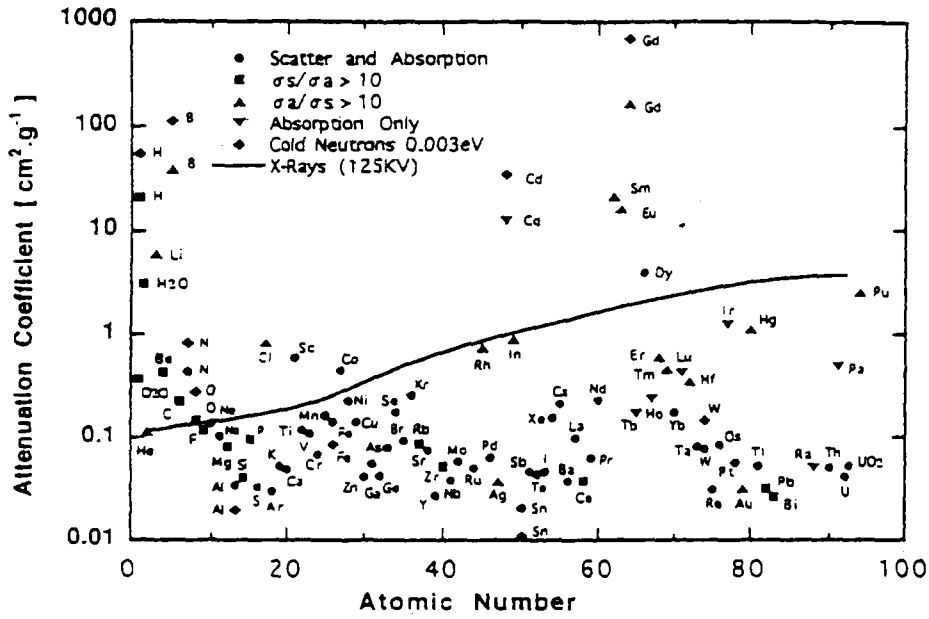

Fig.1 Mass attenuation coefficients of thermal neutrons and X-ray in various elements.

quantitative applications. Some attempts have been made to use NR as a tool not only for visualization but also for quantitative measurement. Quantitative utilization can be classified into two categories. The first one is to use the geometrical information extracted from NR images, for example, measurement of particle trajectory and velocity [14], and hold up in a fluidized bed [15]. The second one is to use the attenuation characteristics of neutrons in materials, for instance, measurement of void fraction in multiphase flow [16,17]. For these purposes, quantification method, namely the Σ-scaling method was developed [18]. Concerning the quantification method, it is anticipated that the transmitted neutron profile might be different from what the internal structure of the object accurately projects due to an unparallel incident neutron beam and neutrons scattered in the object. However, since the neutrons scattered in the object could be homogenized and reduced by setting the test section away from the converter, the corrections for the scattered neutrons could be made as an offset like a dark current, and the offset value could be determined by using the total macroscopic cross section of the object (Σ-scaling method) [10]. Moreover, the distance between the test section and the converter, which was needed to eliminate the effect of skewed incident neutron beam and to avoid the influence of scattered neutrons, was estimated [18].

The present paper reviews some of the recent results from our effort [18,24-28].

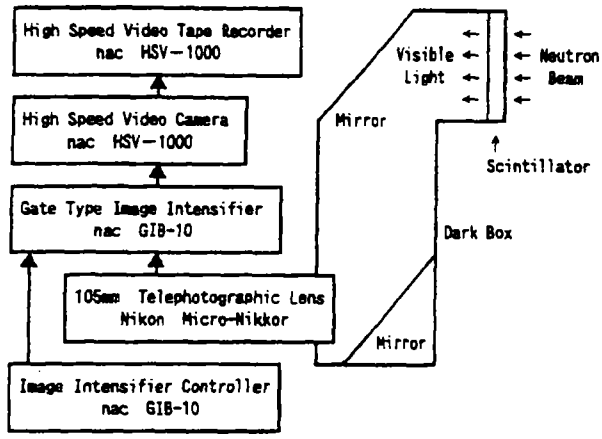

Fig.2 Block diagram of the imaging system for high-frame-rate NR with a steady neutron beam.

2. IMAGING SYSTEM OF HIGH-FRAME-RATE NR

(1) Basic Concept of High Frame Rate NR

Figure 1 shows the mass attenuation coefficients of thermal neutrons and X-rays in various elements [1]. The mass attenuation coefficient of X-rays increases monotonically with the atomic number. On the other hand, thermal neutrons easily penetrate most metals, while they are attenuated well by such materials as hydrogen, water, boron, gadolinium and cadmium. In other words, X-ray radiography takes advantage of the difference in densities, while NR takes advantage of the difference in neutron absorption cross-sections. Therefore, it is clear that NR is more suitable for observing the behavior of a neutron absorbing fluid in a metallic duct.

The block diagram of the imaging system for high-frame-rate NR with a steady neutron beam is

shown in Fig.2. Here, the test section is set up in front (right hand side) of the scintillator. When the neutron beam penetrates two-phase flow in the test section, the beam is attenuated in proportion to the water layer thickness along its path. Thus the neutron beam projects the image of two-phase flow. The neutron beam which conveys the image of two-phase flow is changed into an optical image by the scintillator. The luminous intensity of the optical image is then increased by an image intensifier to obtain a better image. After the image is enlarged with a telephotographic lens, it is detected with a high-speed video camera. The quality of the obtained image can be improved by using an image processing system consisting of an image memory and image processor. The following are necessary conditions to achieve the high-frame-rate NR:

a. a high flux research reactor producing a steady neutron beam,
b. a highly-sensitive scintillator with a short light-decay constant,
c. a high-speed video system with a long recording time,
d. high sensitivity camera with a high performance image intensifier.

An outline of each item is discussed in the following sections.

(2) Neutron Source

It is said that the present highest thermal neutron flux available from existing NR facilities is on the order of 10^8 n/cm^{2}s at the imaging plate. The Japan Research Reactor 3M (JRR-3M) of JAERI, which is one of a few facilities producing neutron flux on the order of 10^8 n/cm^{2}s at the imaging plate, was used as a neutron source in this study. The JRR-3M is a pool type research reactor operated at 20 MW, which has three NR facilities: TNRF-1 for highly radioactive objects, TNRF-2 for non-radioactive objects, and CNRF which uses cold neutrons instead of thermal neutrons. TNRF-2 was used in the present experiment. It has a divergent type collimator and the thermal neutron flux at the imaging plate is 1.5×10^8 n/cm^{2}s. The area of the sight is (V)255×(H)305 mm and the L/D ratio of the vertical and the horizontal directions are 153 and 176, respectively. The L/D ratio is a measure of resolution of the NR system, where L is the distance from the entrance aperture to the imaging plate and D is the diameter of the entrance aperture. A NR facility with the L/D ratio larger than 100 has good performance charac-teristics. Thus it is expected that high quality images will be obtained using the JRR-3M.

(3) Scintillator [19,24]

The converter/scintillator to be used in high-frame-rate NR should have characteristics of a high light yield, high resolution, short light decay time. Since rare earth scintillators of gadolinium compounds have a long light-decay time and glass scintillators have a low light-yield, these are not applicable to high-frame-rate NR. Only zinc sulphide (ZnS) scintillators mixed with lithium fluoride (^{6}LiF) meet the above three conditions. The NR converter (^{6}LiF/ZnS:Ag) supplied by Kasei Optonix was selected as a scintillator. Compared to the gadolinium metal scintillator, the sensitivity of this scintillator is 100 times larger and its sharpness is about 90%. Moreover, this scintillator has a light-decay constant smaller than a few ten μs which could be applicable to high-frame-rate NR at the recording speed of 10,000 to 25,000 frames/s. Kasei Optonix NR converter and Nuclear Enterprises 426 scintillator has the highest light-yield.

(4) High-Speed-Camera

The purpose of developing high-frame-rate NR with a steady neutron beam is to visualize rapid phenomena for a long time period. Therefore, a high-speed video with a long recording time should be used, although the sensitivity is also important. Thus a high-speed video system, nac-HSV-1000 system, was selected in the present experiment. This system can record images for 21 minutes at 1000 frames/s with an ordinary VHS video tape with the recording time of 180 minutes at the normal speed. The shuttering speed of the built-in rotary shutter is 1/10,000 s and the relative sensitivity is 50 in ISO. The resolution is 350 × 480 pixels.

(5) Image Intensifier

An image intensifier, nac GIB-10, was selected in view of the best matching with HSV-1000. This image intensifier belongs to the category of the fourth generation. The amplification rate is about 100,000 at its maximum and the gate time can be controlled to be from 100 ns to continuous mode. The resolution is 23 line-pairs/mm. Although the amplification rate can be increased by using the image intensifier with double micro-channel plates (MCP), GIB-M2P, the resolution and the image quality may be reduced in return. Therefore, the image intensifier with a single MCP was used in the two-phase flow experiment, while that with GIB-M2P was used in the molten metal-water interaction experiment in which high speed phenomena may be observed.

3. THE Σ-SCALING METHOD FOR VOID FRACTION MEASUREMENT

(1) Basic Idea of the Σ-scaling method

The flux of incident neutron ϕ_{th} is attenuated in the water and the aluminum of the test section, thus

$$\phi = \phi_{th}\exp(-\Sigma_G\delta_{MG} - \Sigma_L\delta_{ML} - \Sigma_T\delta_T) + \phi_S \quad (1)$$

where ϕ and ϕ_S denote the total neutron flux falling on the converter and scattered neutron component, respectively. Σ and δ denote the macroscopic cross section and thickness of the material, respectively. Subscripts G, L, MG, ML and T denote the single-phase gas, single-phase liquid, gas in the mixture, liquid in the mixture and the test section, respectively. Ignoring the neutron absorption in the gas phase, the measured gray levels G are given by the following equations for the gas-filled, liquid-filled, and two-phase-mixture-filled test sections.

$$\bar{G}^0_G = C\phi_{th}\exp(-\Sigma_T\delta_T) + G_0 \ , \quad (2)$$

$$\bar{G}^0_L = C\phi_{th}\exp(-\Sigma_L\delta_L - \Sigma_T\delta_T) + G_0 \ , \quad (3)$$

$$\bar{G}^0_M = C\phi_{th}\exp(-\Sigma_L\delta_{ML} - \Sigma_T\delta_T) + G_0 \ , \quad (4)$$

where G_0 is the offset term which consists of scattered neutron component, G_S, and dark current, G_D; $G_0 = G_S + G_D$. The tilde (~) denotes that the gray levels of the images were normalized, i.e. by matching the reference brightness at the vacant space outside the test section. The scattered neutron component, G_S, consists of neutrons scattered in the test section, G_{SM}, and those scattered in the surrounding background objects, G_{SS};

$$G_S = G_{SM} + G_{SS} = C(\phi_{SM} + \phi_{SS}) \ . \quad (5)$$

It should be noted here that generally, G_{SM} depends on the mixture flowing in the test section, while G_{SS} could be considered to be spatially flat. More discussion will be given on this point later.

The void fraction, α, is obtained by

$$\alpha = 1 - \frac{\delta_{ML}}{\delta_L} = \frac{\ln\left(\frac{\bar{G}_L}{\bar{G}_M}\right)}{\ln\left(\frac{\bar{G}_L}{\bar{G}_G}\right)} = \frac{\ln\left(\frac{\bar{G}^0_L - G_0}{\bar{G}^0_M - G_0}\right)}{\ln\left(\frac{\bar{G}^0_L - G_0}{\bar{G}^0_G - G_0}\right)} \ . \quad (6)$$

The offset term, G_0, can be determined using the gray levels obtained from the liquid-filled and gas-filled test sections:

$$G_0 = G_S + G_D = \frac{\bar{G}^0_L - \bar{G}^0_G\exp(-\Sigma_L\delta_L)}{1 - \exp(-\Sigma_L\delta_L)} \ . \quad (7)$$

By determining the offset term, G_0, based upon the total macroscopic cross section, Σ, quantitative data could be derived from the relative gray levels. Thus this method is called the Σ-scaling method. For the Σ-scaling method to be applicable to fluids with unknown void fraction, the scattered neutron component, G_S, should be spatially uniform, so that G_0 is independent of spatial position and could be simply treated as a constant offset. As G_{SS} could be considered to be spatially independent, spatially flat G_S could be achieved when ϕ_{SM} is spatially flat, or if not, $\phi_{SM} \ll \phi_{SS}$. To achieve a spatially flat G_S, ϕ_{SM} is reduced and smoothed by taking an appropriate distance, L', between the test section and the converter. This distance is currently being experimentally estimated to be greater than the width of the test section. When the distance is too large, the skew of the incident neutron beam causes the image to appear blurry, especially in the vicinity of the material boundary. This upper limit of L' could be given by the product of the spatial resolution and the L/D ratio of the NR facility. Thus the appropriate range of L' to be used in the Σ-scaling method should be an optimum value that takes into account the above two conditions.

(2) Measurement Error due to Statistical Variation of Neutrons

Since the measurement of neutrons generated by a random process is affected by statistical variation, the measurement error increases with recording speed [29]. As the measurement error is usually given by the standard deviation, the relative measurement error E is given as a function of the neutron fluence F by the equation:

$$E = \frac{\sqrt{F}}{F} \ . \quad (8)$$

The neutron fluence per pixel area in the image sensor is given by

$$F = \phi_{th}\exp(-\Sigma_w\delta_w)R^2\Delta t \ , \quad (9)$$

where R is the spatial resolution of the image, namely, the real scale projected in a pixel [cm/pixel], Δt is the measuring time or exposure time, and subscript w denotes water. Here the neutron attenuation in the aluminum wall of the duct is neglected.

By integrating N consecutive frames, the relative measurement error in Eq.(8) could be decreased by $1/\sqrt{N}$, thus:

$$E' = \frac{\sqrt{F/N}}{F} . \quad (10)$$

Therefore, the following relatiohship is obtained between the mesurement error E' and the maximum recording speed M:

$$M = \frac{1}{t} = \phi_{th} \exp(-\Sigma_L \delta_{ML} - \Sigma_T \delta_T) R^2 E'^2 N . \quad (11)$$

From this equation, the measurement error at 30 frames/s becomes 0.23% for air-water two-phase flow in the present rectangular test section under the following assumptions: the water layer thickness is 2.4 mm; the attenuation in the aluminum test section can be neglected; the spatial resolution is 0.3 mm; and N=100. If the recording speed is increased to 1000 frame/s, then the measurement error becomes 5.8 times larger than that at 30 frames/s under otherwise the same condition.

(3) Measurement Error due to Limited Gray Scale

The measurement error due to limited gray scale was studied previously [29]. Here we assume for simplicity an ideal imaging system which suffers neither noise in the brightness signal nor image shading, and that the effect of scattered neutrons can be nelgelcted. The attenuation of neutrons in the test section is expressed by Eq.(1) which can then be simplified by the following equation for air-water flow in a rectangular duct:

$$\phi = \phi_{th} \exp(-\Sigma_w \delta_w) . \quad (12)$$

Here the attenuations in the duct wall and the air are neglected. The penetrated neutrons are then converted to visible light by the converter, detected by a highly sensitive camera, and transformed to discrete gray levels as Eq.(4) which can be simplified as:

$$G = C\phi_{th} \exp(-\Sigma_w \delta_w) + G_0 . \quad (13)$$

Due to this digitization, the gray level, which we call hereafter a gray scale, becomes a discrete function of water layer thickness. This means that a constant value of gray scale is specified for a range of water layer thickness. In other words, this causes an error in determining the water layer thickness based on the measured gray scales. Letting the gray scale for $\delta_w=\delta_c$ be G_{low} and that for $\delta_w=0$ be G_{upp}, then we obtain:

$$C\phi_{th} = \frac{G_{low} - G_{upp}}{\exp(-\Sigma_w \delta_c) - 1} , \quad (14)$$

$$G_0 = \frac{G_{upp} \exp(-\Sigma_w \delta_c) - G_{low}}{\exp(-\Sigma_w \delta_c) - 1} . \quad (15)$$

Rearranging Eq.(13), we obtain the expression for water layer thickness:

$$\delta = \frac{1}{\Sigma} \ln\left(\frac{C\phi_{th}}{G - G_0}\right) . \quad (16)$$

Then the resolution, $\Delta\delta$, between i-th and (i+1)-th water layer thicknesses, δ_i and δ_{i+1}, is given by i-th and (i+1)-th gray scales, G_i and G_{i+1}, as follows:

$$\Delta\delta = \delta_i - \delta_{i+1} = \frac{1}{\Sigma_w} \ln \frac{G_{i+1} - G_0}{G_i - G_0} . \quad (17)$$

Finally, the measurement error, E_i due to limited gray scale becomes:

$$E_i = \frac{\Delta\delta}{\delta_i} = \frac{\delta_i - \delta_{i+1}}{\delta_i} = \frac{\ln \frac{G_{i+1} - G_0}{G_i - G_0}}{\ln \frac{C\phi_{th}}{G_i - G_0}} . \quad (18)$$

The gray scale, G_i takes an integer value and the water layer thickness is a logarithmic function of the gray scale. Numerical calculation using the above equations lead to the following conclusions [30]: if one uses an image processing system with a limited band of gray scales, the measurement error may not be negligible at very high and very low void fraction regions; In measuring air-water two-phase flow in a rectangular duct with a gap smaller than 9 mm, if the gray scale can be larger than 100, the measurement error due to the limited gray scale is within 5% except in the annular flow region in which the void fration is larger than 90%.

4. EXPERIMENT

Two experiments were performed by using the above-described imaging system. One was a

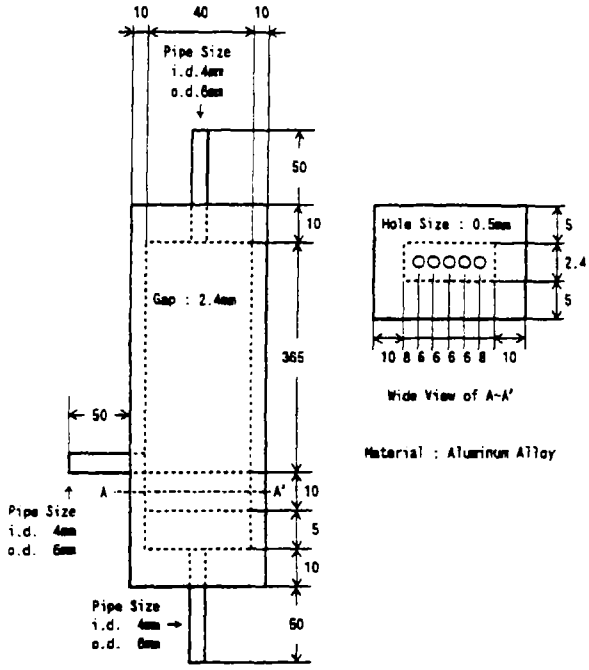

Fig.3 Schematic drawing of the test section used in the two-phase flow experiment.

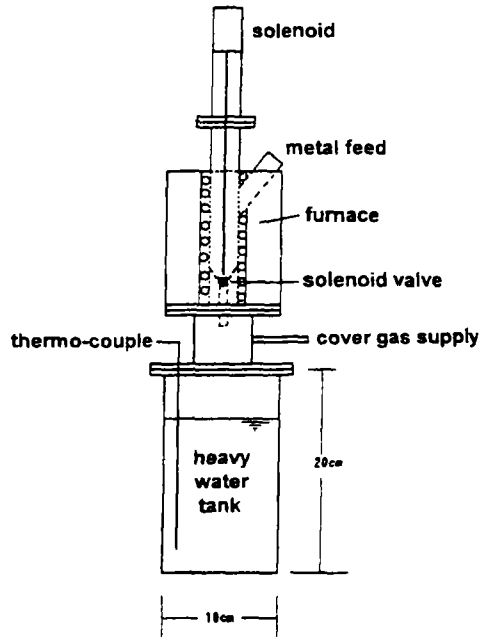

Fig.4 Test rig for the molten-metal-water interaction experiment.

visualization study determining the feasibility of high-frame-rate NR with a high-speed video system. The other was to examine the proposed method of extracting quantitative information, i.e. void fraction, and to study the effects of scattered neutrons and skew of the neutron beam. In the former, an air-water two-phase flow in a rectangular duct (2.4 mm in gap and 40 mm in width) made of aluminum alloy and the behavior of Wood's metal drops in a heavy water pool were visualized. The gap 2.4 mm was chosen to represent the coolant channel of an MTR type fuel element. It should be noted also that if one uses water as the working fluid, the measurement error by the Σ-scaling method becomes large due to the large neutron attenuation when the water layer thickness is larger than several milimeters [29].

In the latter experiment, a triple tube test section was used as a benchmark to verify the quantification method, i.e. Σ-scaling method [18]. The triple tube test section was chosen to simulate several values of void fraction as well as radial void distributions by filling and unfilling the gaps. The void fraction measurement using the NR method was also verified in comparison with other methods such as optical and probe methods.

(1) Two-Phase Flow Experiment

The test section was a rectangular duct made of an aluminum alloy with 2.4 mm gap, 40 mm width and 365 mm length. The schematic drawing is shown in Fig.3. The flow in the test section was a vertical upward air-water flow. Purified water was circulated in the loop by a centrifugal pump, and the air was supplied by an air compressor through five small holes with 0.5 mm diameter in the air-distributor at the bottom of the test section. After flowing through the test section, the air was discharged into the atmosphere.

(2) Molten Metal-Water Interaction Experiment

The test rig consisted of a furnace and a test section as shown in Fig.4. The furnace could heat Wood's metal to 600°C with a 1kW electric heater. The test section was a rectangular tank made of an aluminum alloy (water layer thickness 30mm and width 200mm). In this experiment, visualization of molten metal-water interaction was tested at recording speeds from 500 to 1000 frames/s, in which we intended to observe molten metal, bubble and water. For this purpose, heavy water and Wood's metal were used. Heavy water was used because light water might attenuate neutrons too much. Wood's metal was used because of its large neutron absorption, which would produce good contrast against heavy water in resultant neutron radiography. Thus heavy water at the room temperature was used in the tank. Molten Wood's metal heated to 600°C was dropped into the tank by opening the solenoid valve mounted at the bottom of

Table 1 Dimensions of the triple-tube test section.

Tube	Measured Dia.	Symbol	Center Pos.	Symbol
Inner	1.48 mm I.D.	r_1	0.00 mm	x_1
Tube	2.02 mm O.D.	r_2	0.00 mm	x_2
Center	3.05 mm I.D.	r_3	-0.357 mm	x_3
Tube	4.05 mm O.D.	r_4	-0.357 mm	x_4
Outer	4.92 mm I.D.	r_5	-0.446 mm	x_5
Tube	6.00 mm O.D.	r_6	-0.446 mm	x_6

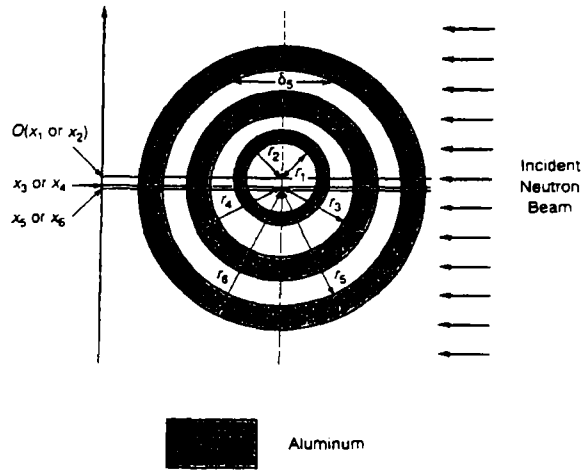

Fig.5 Cross sectional view of the triple tube test section.

the furnace so that molten metal was dropped in a jet or lumps.

(3) Triple Tube Experiment

The cross sectional view of the triple tube test section made of aluminum is shown in Fig.5. The tubes were not exactly concentric because of the fabrication error. The dimensions are shown in Table 1. The length of the test section was 250 mm. The aluminum walls of the inner and center tubes are considered to be void in view of neutron absorption. Seven kinds of void fractions, namely 0.371, 0.462, 0.587, 0.678, 0.694, 0.784 and 0.910 can be obtained by combining the gas-filled and liquid-filled gaps.

5. RESULTS AND DISCUSSION

(1) Visualization of Flow Regimes

Original images of typical two-phase flow regimes in the rectangular duct taken at the speed of

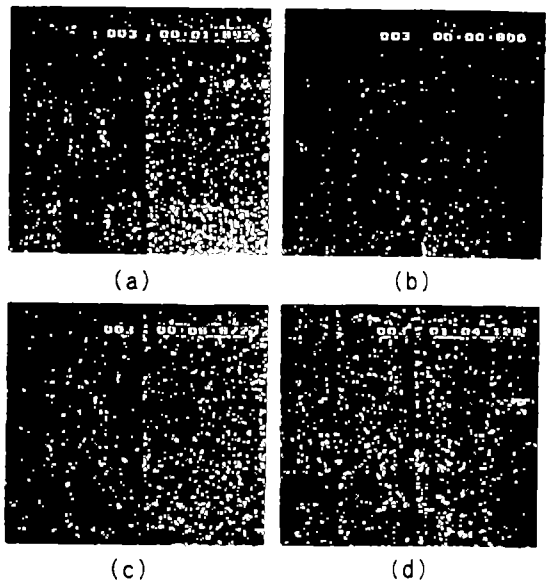

Fig.6 Images of air-water two-phase flows in a rectangular duct taken by the high-frame-rate NR at 500 frames/s: (a) bubbly flow, (b) slug flow, (c) churn flow, (d) annular flow.

500 frames/s are shown in Fig.6. The flow regimes (a), (b), (c) and (d) are identified as bubbly, slug, churn and annular flows, respectively. The rising behavior of the bubbles, the shape of a slug bubble, disturbances in the air-water interface and growing waves on the liquid film can be clearly observed. Consecutive images of a typical annular flow taken at the speed of 250 frames/s are shown in Fig.7. To emphasize the motion of the interface, the images are shown every 8 ms. Since the waves move upward, the flow regime demonstrated in this figure is considered to be annular flow. Thus it is seen that the quality of the obtained NR images is sufficient to discriminate flow regimes.

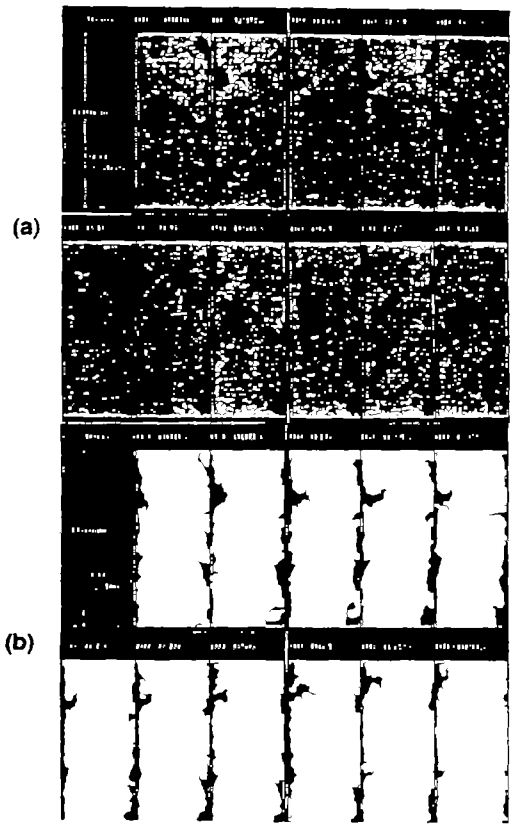

Fig.7 Consecutive images of a typical annular flow taken at the speed of 250 frames/s: (a) Original images, (b) Processed images (binary-value transformation).

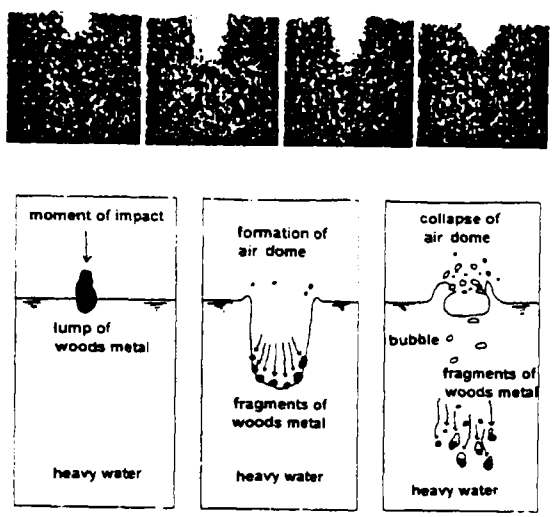

Fig.8 Consecutive images and the schematic sketch of the behavior of Wood's metal dropped into heavy water taken at the speed of 500 frames/s.

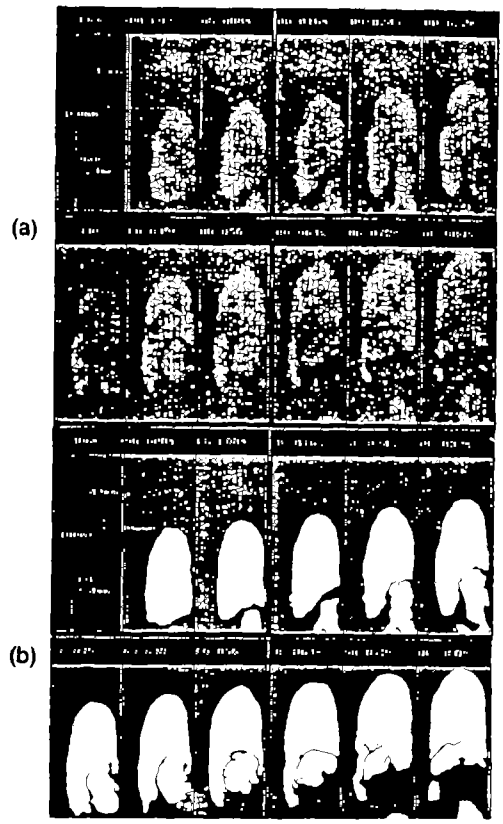

Fig.9 Consecutive images of a typical slug flow taken at the speed of 250 frames/s: (a) Original images, (b) Processed images (binary-value transformation).

Figure 8 shows consecutive images of the behavior of Wood's metal dropped into heavy water. In this figure it is demonstrated that the behavior of molten Wood's metal inside the bubble could be visualized at a speed of 500 frames/s. One of the advantages of using the neutron radiography is that the behavior of molten metal inside a bubble can be visualized without the deformation of the image, while it is difficult due to the reflection at the bubble surface if one uses an optical method. From this experiment, it was demonstrated that the fragments with a size of a few milimeter and larger in diameter could be detected by this method, and when steam explosion occurred, a cloud of small particles of molten metal was observed.

(2) Quantitative Data Obtained by Image Processing

Rising velocity of slug bubbles Consecutive images of a typical slug flow in the rectangular duct taken at the speed of 250 frames/s are shown in Fig.9(a) and the corresponding processed (binary)

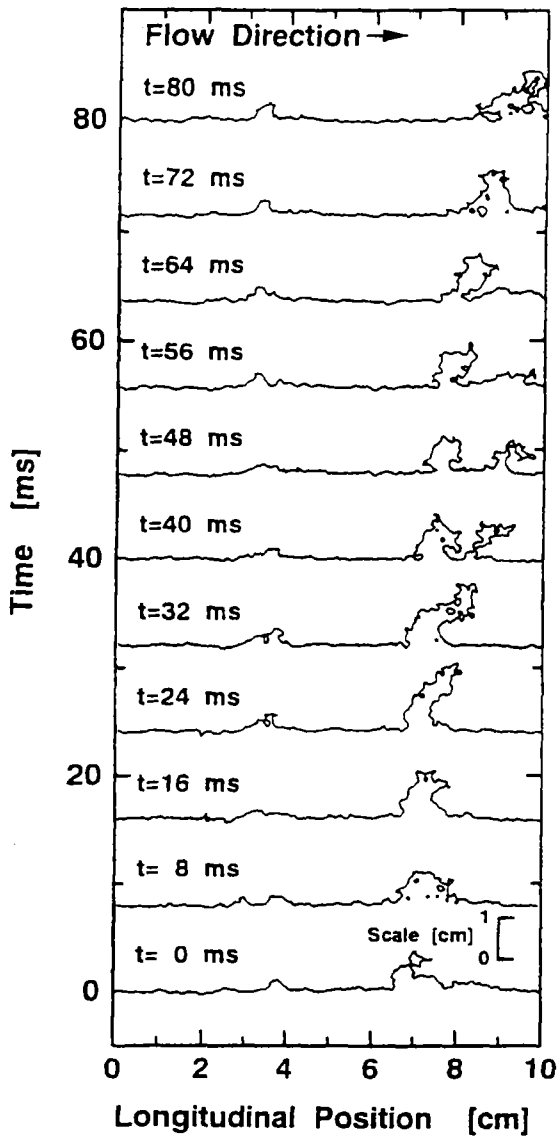

Fig.10 Motion of a disturbance wave on the annular liquid film depicted by image processing (edge detection).

images are shown in Fig.9(b). Thus appropriate processing enhances the image and delineates the flow regime. In those images, the vertical and horizontal lengths of the frame are 100 and 40 mm, respectively. The coalescence of a slug bubble with a following bubble in the wake can be clearly observed. Since the slug bubble moved 42 mm upward in 80 ms, the rising velocity can be estimated to be 52.5 cm/s. In this manner the moving velocity of bubbles can be directly measured from the consecutive images.

Wave Height, Interfacial Length and Interfacial Area in Annular Flow The wave height in this case is defined as the distance between the air-water interface and the side wall. Since the gap of the test section is very narrow, the flow could be considered as two-dimensional. Therefore, the interfacial length in this paper indicates the path of the interface, and the interfacial area is calculated from the interfacial length and the gap. The following image processing techniques were used to obtain the aforementioned quantities:

a. shading correction: dividing the gray level of two-phase flow image by that of the image of the empty test section,
b. smoothing: applying the averaging filter to the image (this filter is to reduce the random noise by averaging the gray level of the objective pixel and its neighboring 8 pixels,
c. binary-value transformation: applying the binary-value transformation to the image after determining the appropriate threshold level,
d. noise reduction: eliminating small isolated irregular pixels in the image,
e. edge detection: applying the Laplacian filter to the binary image,
f. measurements: counting the pixel number after scaling the pixel length to the real scale.

In Fig.7 (a) and (b), consecutive images of annular flow taken at the speed of 250 frames/s and corresponding processed (binary-value transformed) images, respectively, were shown. The motion of interface waves on the annular liquid film could be clearly extracted if one applies edge detection to the images in Fig.7(a). The results are shown in Fig.10. It should be noted here that the location of the interface determined by the present method depends to some extent on the filter used and its discrimination level which was determined rather empirically. However, if the discrimination level is appropriate one, then the location of the interface could be determined reasonably well, at least, to delineate the behavior of the interface, which can be seen by comparing Figs.7 and 10. The wave height and the interfacial length and area were also obtained and have been described previously [25].

Void Fraction The Σ-scaling method was tested with known void profile produced by the triple tube test section. Figure 11 shows the comparison between designed and measured profiles of the water-layer thickness across the triple tube test section. Here L' is the distance between the test section and the converter. The solid line and circles denote designed (simulated) and measured water-layer thicknesses, respectively. It can be seen from the figure that agreement is good, which indicates the validity of the present quantification method. It is noted also that the measured and calculated average void fractions agree well with each

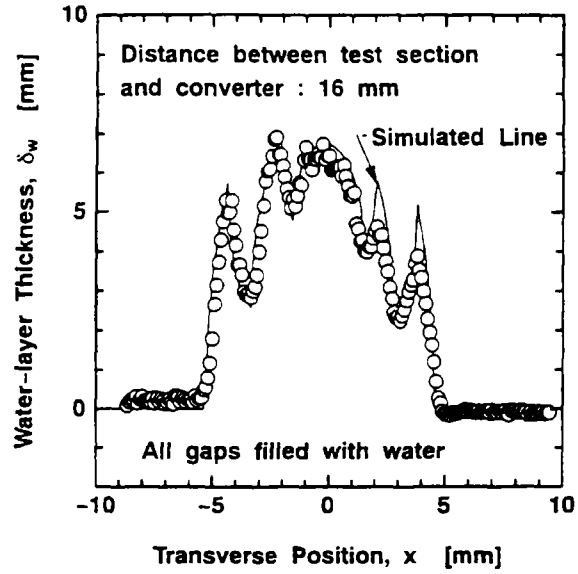

Fig.11 Comparison between the designed and measured profiles of water thickness for the triple tube test section with all the gaps filled with water.

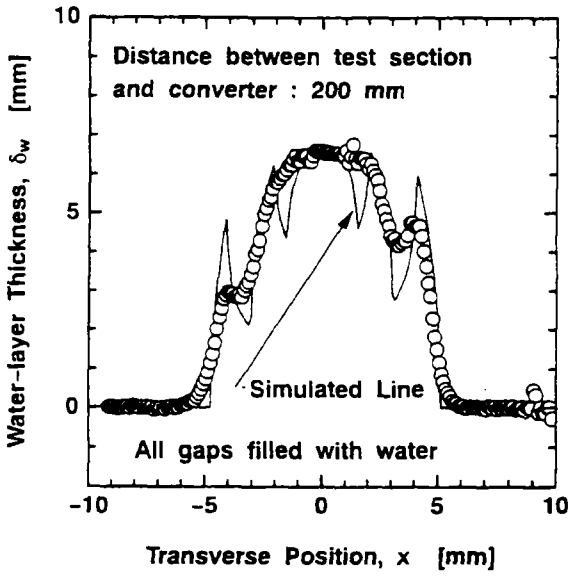

Fig.12 Effect of the distance between the test section and the converter on the water-layer thickness profile measured by the Σ-scaling method.

other. The data shown in Fig.11 was taken with the test section placed at the distance of 16 mm from the converter. As discussed earlier, the image becomes blurry due to the skew of the incident neutron beam if the test section is placed too far from the converter. An example for this is shown in Fig.12

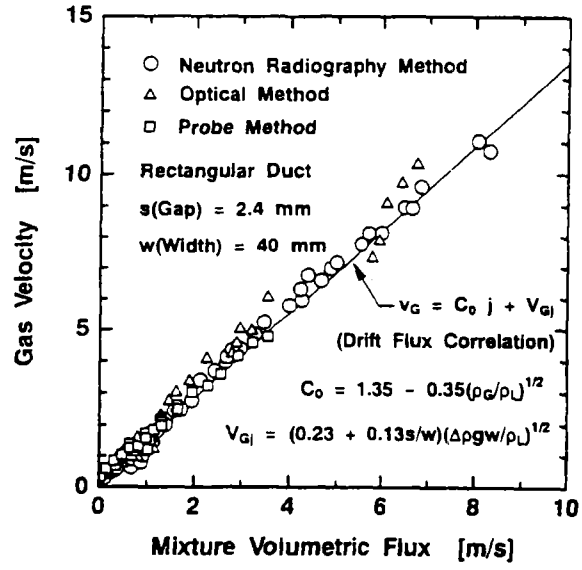

Fig.13 Comparison of the measured void fractions taken by the real-time NR, optical and conductance methods with the drift flux correlation.

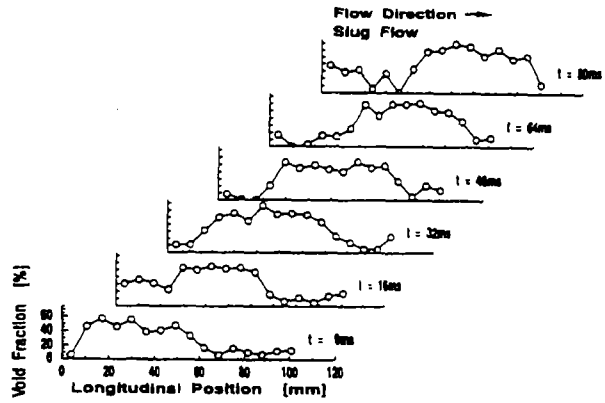

Fig.14 Temporal variation of void profile in slug flow along the flow direction.

which was taken at the distance of 200 mm from the converter.

Moreover, to confirm this method for the void fraction of two-phase flow in a rectangular duct, gas velocities calculated from the void fractions measured by the NR method are compared with those by the optical and conductance probe methods [16], as shown in Fig.13. Since the measured values taken by the high-frame-rate NR are particularly affected by the statistical variation of neutrons as discussed previously, the integrated image of the images obtained by the real-time NR with the recording speed of 30 frames/s instead of the high-frame-rate NR was used here.

In Fig.13, the solid line indicates the prediction

by the drift flux correlation for a rectangular duct [31,32]. It is shown that the measured values are consistent and correlated well using the drift flux correlation. The measurement error by the NR method is estimated to be within 5%.

Spatial Distribution and Temporal Variation of Void Fraction It is possible to calculate various types of average void fraction from Eq.(6). The time-averaged local void fraction can be measured from the images integrated with time by the image-totalizer. The space-averaged void fraction in the entire test section and the cross section of the channel can be obtained by averaging the void fraction in the region of interest. The temporal variation of the void profile in the flow direction, which was measured by averaging the void profile across the channel at intervals of 6.45 mm along the flow direction, is shown in Fig.14. The original images used here are those shown in Fig.9(a) for a slug flow. It can be seen from Fig.14, that the region where the void fraction is high moves upward in accordance with the rise of the slug bubble and two peaks in void profile merged into one peak, which corresponds to the coalescence of two bubbles, as mentioned previously. Thus it is confirmed that the present high-frame-rate NR system combined with image processing technique can be a useful tool for visualizing and measuring fluid phenomena.

6. SUMMARY

To apply the neutron radiography (NR) technique to fluid research, a high-frame-rate NR with a steady thermal neutron beam was developed by combining up-to-date technologies for neutron source, scintillator, high-speed video and image intensifier. This imaging system has many advantages such as a long recording time, high-frame-rate (up to 1000 frames/s) imaging and no need for a trigger signal.

Visualizations of air-water two-phase flow in a metallic rectangular duct and molten metal-water interaction were achieved at the recording speeds of 250, 500 and 1000 frames/s. The qualities of the consequent images were sufficient to observe the flow pattern and to measure the flow characteristics.

It was demonstrated that some characteristics of two-phase flow could be measured using the present imaging system. Image processing techniques enabled measurements of those characteristics. By utilizing geometrical information extracted from the NR images, data on flow regime, bubble rise velocity, and wave height and interfacial area in annular flow were obtained. By utilizing attenuation characteristics of neutrons in materials, measurements of void profile and average void fraction were performed. The present quantification method, i.e. Σ-scaling method was verified against known void fraction profiles produced by the triple tube test section as well as the data taken by the conventional methods.

From these, it was confirmed that this new technique may have significant advantages both in visualizing and measuring rapid fluid phenomena when conventional methods such as the optical methods and X-ray radiography cannot be applied.

ACKNOWLEDGEMENTS

The authors would like to acknowledge Messrs. M. Matsubayashi and A.Tsuruno (Department of Research Reactor, Tokai Establishment, JAERI) for their assistance in part of the experiment. Part of this work was performed as the joint research program with JAERI.

REFERENCES

[1] P. von der Hardt and H. Röttger, Eds., *Neutron Radiography Handbook*, D. Reidel, Dordrecht, Holland (1981).

[2] J.P. Barton, Proc. 5th Int. Symp. Advanced Nuclear Energy Research – Neutrons as Microscopic Probes, Mito, Japan, March 10-12, 1993, JAERI-M93-228, Vol.1, p.125 (1993).

[3] G. Costigan et al., Int. Workshop on Post-Dryout Heat Transfer, Salt Lake City, USA 2-101 (1984).

[4] G.F. Hewitt et al., NUREG/CP-0058 (1985).

[5] G. Costigan et al., AERE-R-12561 (1987).

[6] K. Mishima et al., *Proc. Japan-US Seminar on Two-Phase Flow Dynamics, Ohtsu, Japan, Paper No.C3 (1988); Dynamics of Two-Phase Flow* (Eds. O.C. Jones and I. Michiyoshi), CRC Press, p.142 (1992).

[7] T. Hibiki et al., *Neutron Radiography (4)* (J.P. Barton, Ed.): Proc. 4th World Conf. Neutron Radiography, San Francisco, California, May 10-16, 1992, p.317, Gordon & Breach, Yverdon, Switzerland (1994).

[8] S.S. Glickstein, et al., ANS/ENS 1992 Int. Conference, Chicago, USA (1992).

[9] B.S. Carlisle et al., Proc. 4th Int. Topical Meeting on Nucl. Thermal Hydraulics m Operation & Safety, Taipei, Taiwan 2 (1994) 43-B-1.

[10] T. Fujii et al., Trans. Jpn Soc. Mech. Engrs. (Ser.B)m 57 (1991) 256.

[11] D. Sathianathan, PhD Thesis, Pennsylvania State Univ. (1990).

[12] J.S. Chang et al., Proc. 4th Int. Topical Mtg. on Nucl. Reactor Thermal Hydraulics, NURETH-4, Karlsruhe, Germany (1989) 413.

[13] N. Takenaka, T. Fujii, A. Ono, K. Sonoda, S.

Tazawa and T. Nakanii, ibid., p.355 (1992).
[14] F. Ogino, M. Kamata, K. Mishima, S. Fujine, K. Yoneda, and K. Kanda, ibid., p.339 (1994).
[15] S. Chiba, K. Idogawa, Y. Maekawa, H. Moritomi, N. Kato and T. Chiba, Fluidization VI, Proc. Int. Conf. Fluidization, Banff, Alberta, Canada, May 7–12, 1989, p.523, AIChE (1989).
[16] K. Mishima, T. Hibiki and H. Nishihara, Int. J. Multiphase Flow, 19 (1993) 115.
[17] T. Hibiki, K. Mishima, H. Nishihara and T. Motomura, Annu. Rep. Res. Reactor Inst. Kyoto Univ., 36 (1993) 34.
[18] K. Mishima and T. Hibiki, Nucl. Sci. Eng. 124 (1996) 327.
[19] R.H. Bossi, A.H. Robinson and J.P. Barton, Nucl. Technol., 59 (1982) 363.
[20] J.M. Cimbala, D.E. Hughes, S.H. Levine, and D. Sathianathan, Nucl. Technol., 18 (1988) 435.
[21] M. Matsubayashi and A. Tsuruno, *Neutron Radiography (4)* (Ed. J.P. Barton): Proc. 4th World Conf. Neutron Radiography, San Francisco, U.S.A., May 10–16, 1992, p.415, Gordon & Breach, Yverdon, Switzerland (1994).
[22] F.M. McCrory, J.G. Kelly, D.A. Tichnor and A.A. Verberkmoes, ibid., p.423 (1994).
[23] R. Tanaka and K. Ando, Optronics, 12 (1991) 73 (in Japanese).
[24] T. Hibiki, K. Mishima, K. Yoneda, S. Fujine, A. Tsuruno and M. Matsubayashi, Nucl. Instrum. Methods in Phys. Res A351 (1994) 423.
[25] T. Hibiki, K. Mishima and M. Matsubayashi, Nucl. Technol., 110 (1995) 422.
[26] K. Mishima, T. Hibiki, S. Fujine, K. Yoneda, A. Tsuruno, M. Matsubayashi and M. Sobajima, Trans. Jpn. Soc. Mech. Engrs. Ser.B, 61[591] (1995) 3959 in Japanese.
[27] K. Mishima and T. Hibiki, Trans. Jpn. Soc. Mech. Engrs. Ser.B, 62[593] (1996) 137 in Japanese.
[28] K. Mishima and T. Hibiki, Exper. Therm. Fluid Sci. 12 (1996) 461.
[29] T. Hibiki and K. Mishima, Nucl. Instr. Meth. Phys. Res. A369 (1996) 186–194.
[30] T. Hibiki and K. Mishima, Trans. Jpn. Soc. Mech. Engrs. Ser.B, 62[597] (1996) 1782–1787 in Japanese.
[31] P. Griffith, ASME Preprint, 63-HT-20 (1963).
[32] M. Ishii, ANL Report ANL-77-47 (1977).